Atomic structure of nanometer-sized amorphous TiO_2

Hengzhong Zhang,* Bin Chen, and Jillian F. Banfield
Department of Earth and Planetary Science, University of California–Berkeley, Berkeley, California 94720, USA

Glenn A. Waychunas
Earth Sciences Division, Lawrence Berkeley National Laboratory, Berkeley, California 94720, USA
(Received 17 September 2008; revised manuscript received 19 November 2008; published 16 December 2008)

Amorphous titania (TiO_2) is an important precursor for synthesis of single-phase nanocrystalline anatase. We synthesized amorphous titania by hydrolysis of titanium ethoxide at the ice point. Transmission electron microscopy examination and nitrogen gas adsorption indicated that the particle size of the synthesized titania is ~2 nm. Synchrotron wide-angle x-ray scattering (WAXS) was used to probe the atomic correlations in this amorphous sample. Atomic pair-distribution function (PDF) derived from Fourier transform of the WAXS data was used for reverse Monte Carlo (RMC) simulations of the atomic structure of the amorphous TiO_2 nanoparticles. Molecular-dynamics simulations were used to generate input structures for the RMC. X-ray-absorption spectroscopy (XAS) simulations were used to screen candidate structures obtained from the RMC by comparing with experimental XAS data. The structure model that best describes both the WAXS and XAS data shows that amorphous TiO_2 particles consist of a highly distorted shell and a small strained anataselike crystalline core. The average coordination number of Ti is 5.3 and most Ti-O bonds are populated around 1.940 Å. Relative to bulk TiO_2, the reduction in the coordination number is primarily due to the truncation of the Ti-O octahedra at the amorphous nanoparticle surface and the shortening of the Ti-O bond length to the bond contraction in the distorted shell. The pre-existence of the anataselike core may be critical to the formation of single-phase nanocrystalline anatase in crystallization of amorphous TiO_2 upon heating.

DOI: 10.1103/PhysRevB.78.214106 PACS number(s): 61.46.−w, 61.05.cf, 61.05.cj, 61.43.Bn

I. INTRODUCTION

Titania (TiO_2) is a wide-band-gap (~3.2 eV) semiconductor material with applications in many fields, including medicine, cosmetics, electronics, and chemical engineering. It is known that nanocrystalline anatase has higher photocatalytic activity than other titania nanophases and bulk titania.[1] However, sol-gel synthesis of nanocrystalline titania often results in a mixture of nanoanatase and brookite.[2] Upon heating, the two nanophases transform to rutile.[3–6] In previous work, we developed a two-step route for synthesis of single-phase nanocrystalline anatase.[2] First, amorphous TiO_2 precursor is produced via hydrolysis of titanium ethoxide at a low temperature. Then, heat treatment of the amorphous precursor produces single-phase nanocrystalline anatase.

Thermodynamically, anatase is more stable than rutile at sizes $<\sim 14$ nm.[5,7] However, anatase is only marginally more stable than brookite at sizes $<\sim 11$ nm.[5] This means that in synthesis of nanotitania, brookite is likely to form together with anatase. Considering this, the formation of single-phase nanoanatase (rather than a mixture with brookite) from amorphous titania must be due to the formation kinetics rather than the thermodynamics. Kinetic studies show that the crystallization of nanoanatase from amorphous TiO_2 is initiated at the interfaces between precursor particles.[8] However, it is unclear why the precursor particles preferentially transform to anatase rather than brookite upon heating. Understanding the detailed atomic structure of amorphous titania should help to unveil the transformation mechanism at the atomic level.

In previous studies,[9–15] researchers have used x-ray-absorption spectroscopy (XAS), including x-ray-absorption near-edge structure (XANES) and extended x-ray-absorption fine structure (EXAFS), to investigate the local atomic structures in nanometer-sized amorphous titania or very small titania nanoparticles. For titania particles ~3 nm in diameter, Chen *et al.*[9] reported a coordination number (CN) of 4.8 for Ti atoms based on their EXAFS fitting of the Ti-K-edge XAS data, though they concluded that the Ti sites are largely octahedral (CN=6). Later they showed that, for ~2 nm colloid titania particles, the coordination numbers of Ti atoms are 3.9–5.8 according to the EXAFS fitting.[10] They concluded that distortions in the TiO_2 structure are mainly located on the surface of the particles. EXAFS fitting by Luca *et al.*[11] also showed that small titania xerogels contain Ti in distorted coordination with contracted Ti-O bonds and probably reduced coordination number (CN<6). This seems consistent with EXAFS fitting by Yeung[12] that showed that the Ti-O bond length is 1.93 Å and the coordination number of Ti is 4.5 for a ~3 nm TiO_2 sample. From deconvolution of the pre-edge peaks in the Ti *K*-edge XANES spectra of amorphous mesoporous titania, Yoshitake and co-workers[13,14] concluded that five- and six-coordinated Ti atoms are both present, with their populations being 39% and 61%, respectively. Fernandez-Garcia *et al.*[15] studied the structure of alkoxide-derived amorphous titania using both XAS and pair-distribution function (PDF) methods. Based on the pre-edge feature of the XANES spectra, they deduced that their samples contained five-coordinated Ti atoms. However, their EXAFS fitting showed that the coordination number of Ti atoms is 6.2–6.7, and hence inconsistent with their XAS inference. Petkov *et al.*[16] studied the structures of sol-gel derived, thin film and bulk amorphous titania using x-ray or electron diffraction. Bulk structure models were used in their reverse Monte Carlo (RMC) simulations and from the RMC

they concluded that their samples have brookitelike short-range atomic arrangements.

These previous studies generally pointed out the reduction in the Ti coordination number and the shortening of the Ti-O bond in amorphous (or ultrafine titania particles). However, a detailed atomic view, particularly of the surface, is still lacking. Such knowledge is essential since chemical and physical processes usually either take place on particle surfaces or are initiated there, and most atoms in amorphous nanoparticles are at or near surfaces. In this work, we measured the wide-angle x-ray scattering (WAXS) pattern of alkoxide-derived amorphous titania using a synchrotron-radiation x-ray source, and calculated the atomic pair distribution. Structure models were obtained from RMC by generating the best approximation of the PDF data. By comparing the simulated XAS spectra of these RMC models with the experimentally measured one, we established a structure model that best describes both the WAXS and XAS data. Structural characteristics of the amorphous titania (including surface and interior parts) were further analyzed using this model.

II. EXPERIMENTAL

A. Synthesis and characterization of nanometer-sized amorphous TiO_2

Amorphous titania was prepared by hydrolysis of titanium ethoxide in water at 0 °C (cooled in a bath of ice+water). 29 ml water containing four drops of acetic acid was quickly added to a mixture of titanium ethoxide (21 ml; Acros Organics, New Jersey) and ethanol (25 ml; AAPER Alcohol and Chemical Co., Kentucky) under stirring. The product was centrifuged and washed repeatedly with ethanol first and then with water, and then dried at ~80 °C. The dried sample (in powers) was kept in a sealed glass vial for experimental determinations.

The sample was examined by x-ray diffraction (XRD). A small amount of the sample was lightly ground in acetone in a mortar with a pestle and then dispersed onto a low x-ray scattering background silica plate. The plate was loaded into the sample holder of an x-ray diffractometer (PANalytical X'Pert PRO) operated at 40 kV and 40 mA with a Co $K\alpha$ radiation x-ray source (wavelength, 1.7903 Å). The XRD pattern was collected in the 2θ range of 10°–90° with a scanning rate of 1°/min.

Transmission electron microscopy (TEM) characterization of the microstructure of the sample was done with a Philips CM200 high-resolution transmission electron microscope operated at 200 kV. A TEM specimen was prepared by adding a droplet of titania nanoparticles ultrasonically dispersed in water onto a carbon-coated copper TEM grid, followed by drying in air. The surface area of the sample was determined via the BET (Brunauer, Emmett and Teller) method using nitrogen gas adsorption at 77 K, performed with an Accelerated Surface Area and Porosimetry System (Micrometrics ASAP2010).

B. Wide-angle x-ray scattering

WAXS measurements were performed at the high-energy beamline station 11-ID-C, Advanced Photon Source, Argonne National Laboratory (USA). The x-ray wavelength was 0.107 70 Å and the sample-to-camera distance was ~272 mm. The exact distance was calibrated using diffraction from a CeO_2 standard.

A thin layer of the titania sample was sandwiched between Kapton tape, and attached to a disklike sample holder with an opening for x-ray transmission WAXS measurements. WAXS patterns were acquired at room temperature, with a q (scattering vector) range of 0.3–30 $Å^{-1}$ and a q step size of 0.01 $Å^{-1}$. The WAXS pattern was captured by an image plate detector, with integration of the circularly symmetric scattering pattern about the transmitted beam direction. The WAXS pattern of blank Kapton tape was also acquired for background subtraction. The structure factor $S(q)$ of the sample was derived from the WAXS pattern after suitable data reduction.[17] The atomic PDF G of the titania sample was obtained as a function of radial distance (r) through Fourier transform of the structure factor,[17]

$$G(r) = \frac{2}{\pi}\int_0^\infty q[S(q)-1]\sin(qr)dq. \quad (1)$$

C. X-ray-absorption spectra

Ti K edge (adsorption energy 4966 eV) XANES spectra of bulk anatase, bulk rutile, and the titania sample were measured at Beamline stations 5-BM-D and 20-BM-B, Advanced Photon Source, Argonne National Laboratory (USA). Sample was mixed well with boron nitride (a low-background diluter) in a ratio of 1:9 by weight. The mixture was then transferred into a rectangular-shaped window in a sample holder (~0.5 mm thick), supported behind by Kapton tape. The front of the window was then sealed using another piece of Kapton tape. The measurements were done in transmission mode at room temperature using a Si (111) monochromator. A detuning of around 30% was used for reduction in the contribution from higher harmonics. XANES spectra were collected over the photon energy range of 4965–5020 eV with a step increment varying between 0.2 and 1.4 eV/step. A smaller step increment was used for measuring the pre-edge features of the XAS spectra. The x-ray intensities before the sample, after transmission through the sample, and after subsequent transmission through a standard Ti foil were measured using ionization detectors. Photon energy was calibrated using the absorption spectra of the Ti foil.

III. COMPUTATIONAL MODELING

A. Molecular-dynamics simulations

We used molecular-dynamics (MD) simulations to generate input structures for RMC simulations of the structure of amorphous nano-TiO_2. For the purpose of comparison, we used two sets of interatomic potential functions of TiO_2 in the MD. In the first set, developed by Matsui and Akaogi[18] (MA), each Ti and O atom carries a charge of +2.196 and −1.098, respectively, and the short-range interatomic interactions are described by a Buckingham potential. The MA potentials have been used extensively in simulations of TiO_2

materials (e.g., Ref. 19). In the second set, developed by Kim *et al.*[20] (KIM), each Ti and O atom carries a charge of +2.4 and −1.2, respectively, and the short-range interatomic interactions are described by a Morse potential.

MD simulations were performed using the parallel code DL_POLY.[21] Initial configurations for the MD were structures of 2 and 3 nm (diameter) anatase, brookite, and rutile particles generated by cutting spheres from coordinates of their corresponding bulk phases. Because the as-cut particles were not charge balanced, they were neutralized by removal of excess charged atoms from the outermost surfaces. The MD simulations were carried out in the canonical ensemble (NVT ensemble) at 300 K for MD times of 100–500 ps at a step of $(2.0–5.0)\times 10^{-5}$ ps. The MD times were long enough to ensure that all the MD systems were fully energetically and structurally relaxed, as indicated by the reaching of a steady-state condition in the MD.

B. Reverse Monte Carlo simulations

In a classical Monte Carlo (MC) simulation of the structure of a material, some randomly chosen atoms of the material are moved in random directions for randomly assigned distances. If the energy of the formed new structure is lower than that before the move, the move is "good" and the new structure is accepted. Otherwise, the move is "bad" and the new structure is accepted with a probability of

$$p = \exp\left(-\frac{E_{\text{after}} - E_{\text{before}}}{RT}\right), \tag{2}$$

where E is the molar energy of the material, R is the gas constant, and T is the temperature. After iterating for a sufficient number of MC cycles, the energy of the material decreases to a point where it only fluctuates around a steady value. This energy-minimized structure is considered the most probable. However, in RMC, rather than minimizing the energy of the material, the difference between an observed quantity and a calculated one is minimized through movements of the atoms of a model structure. In this work, the quantity is the atomic pair-distribution function.

In searching for structure models for the amorphous nano-TiO_2 using RMC, we used MD structures as initial input structures for the RMC. This was done because using the neutralized as-cut bulk TiO_2 structure as the initial structure often caused the RMC to fail (because it is generally very far from the actual relaxed structure). The goodness of fit for an RMC structure simulation is measured by the difference between the calculated PDF and the experimental one, χ^2, as defined below,

$$\chi^2 = \frac{\sum_i [I_{i,\text{expt}} - (fI_{i,\text{calc}} + b)]^2}{\sigma^2} = \frac{\text{residual}}{\sigma^2}, \tag{3}$$

where $I_{i,\text{expt}}$ is the experimental PDF intensity at a measured scattering vector q_i, $I_{i,\text{calc}}$ is the calculated PDF intensity at the corresponding scattering vector, σ^2 is a parameter that controls the fraction of bad moves that are accepted, and f and b are, respectively, a scaling factor and a constant that are optimized in each move. In RMC, if a move of atoms causes χ^2 to decrease, then the new structure is accepted (i.e., a good move). Otherwise, if χ^2 increases (i.e., a bad move), the new structure is accepted with a probability of

$$p = \exp\left(-\frac{\chi^2_{\text{after}} - \chi^2_{\text{before}}}{2}\right). \tag{4}$$

After iterating for sufficient RMC cycles, χ^2 will decrease to a point where it fluctuates around a steady value with no further significant structural changes.

In our RMC simulations, for each RMC step about 3% of atoms in the TiO_2 model structure were randomly chosen to move in random directions for random displacements of up to 0.08 Å. Only a small fraction of the atoms were chosen in each random move as use of larger fractions often results in inability to decrease the residual. Using a maximum displacement of 0.08 Å (by numerical tests) also avoided the breaking of Ti-O bonds during each RMC step, a likely unphysical process. Trial-and-error tests showed that $\sigma^2 = 0.01–0.001$ is appropriate for the RMC with our TiO_2 samples. 500 000 RMC cycles were used in each simulation, which guaranteed achievement of a minimum residual.

C. XANES spectra calculation

The Ti K-edge XANES spectra of TiO_2 were calculated using a parallel code FDMNES.[22] Two computational methods are available in FDMNES, the multiple-scattering (MS) method and the finite-difference method (FDM).[23,24] The MS method employs the muffin-tin averaging of the potential needed for the expansion of the wave functions. This method is relatively fast in computation, but may not be accurate at photoelectron kinetic energy close to the point where muffin-tin approximation is done.[23] The FDM method divides a system into small grids and obtains the wave functions by solving the simultaneous quantum-mechanical equations at all the grid points. This removes the assumption of the muffin-tin approximation of the potentials and becomes more accurate in the XANES calculations. However, this method requires significantly greater computational power.

In XANES calculations using FDMNES, the electronic configurations of the atoms of the material are important. The usual initiation technique adopted by FDMNES is to set the appropriate number of "d" electrons, keep the atoms neutral, and put electrons in the large radius $4s$ or $4p$ orbitals for a transition metal.[22] In accordance with this we set the electron configuration of Ti as $[\text{Ar}]3d^1 4s^2 4p^1$, and that of O as $1s^2 2s^2 2p^4$.

For examination of FDMNES, XANES spectra of bulk anatase and rutile were calculated using both the MS and FDM methods, using two atomic cluster radii of 5.6 and 7.0 Å. In the FDM method, crystal symmetry operations were used in the calculations of bulk materials to reduce the computation time. However, the MS method for nanoparticle calculations using structure models obtained from the RMC was preferred due to their lack of symmetry and the large number of atoms involved in the calculations. A XANES spectrum was calculated with a cluster radius of 7 Å for each Ti atom in a TiO_2 nanoparticle (including both surface and interior Ti at-

oms). The spectra of all the Ti atoms were summed and averaged for use as the XANES spectrum of the whole nanoparticle.

For comparison, XANES spectra of typical Ti atoms in a TiO_2 nanoparticle were also calculated using the FDM method using a cluster radius of 4 Å. Larger clusters could not be calculated using available computational power.

D. Structure analysis

The TiO_2 nanoparticle models were analyzed to yield structure characteristics, including the radial-distribution function, coordination numbers as a function of radial distance, bond-length distribution, coordination number of each species, and bond-angle distribution. The partial radial-distribution function g_{ij} is defined as[25]

$$g_{ij}(r) = \frac{1}{4\pi r^2 \rho c_j} \frac{d\langle n_{ij}\rangle}{dr} = \frac{1}{4\pi r^2 N_j} \frac{d\langle n_{ij}\rangle}{dr}, \tag{5}$$

where r is the radial distance, $d\langle n_{ij}\rangle$ is the assemble average of the number of atom j around atom i in a spherical shell with a radius of r and a thickness of dr, ρ is the number density of the material ($\rho = N/\text{volume}$, where N is the total number of atoms), and c_j is the concentration of atom j ($c_j = N_j/N$). g_{ij} represents the probability of finding atom j around atom i at a given radial distance r relative to that at infinitely far away.

The total radial-distribution function g is obtained from

$$g(r) = \sum_{i,j} c_i c_j g_{ij}(r), \tag{6}$$

and represents the probability of finding one particular atom around any other one at a given radial distance, summed over all possible atom pairings.

The number distribution of atom j around atom i, or the coordination number N_{ij} as a function of r is defined as[25]

$$N_{ij}(r) = 4\pi\rho c_j \int_0^r g_{ij}(r) r^2 dr. \tag{7}$$

This function represents the assemble-averaged number of atom j surrounding atom i at a distance r between them. At the position of the first shell of atom j around atom i, N_{ij} equals the conventionally defined coordination number of atom i.

The coordination number of Ti atoms in bulk anatase, rutile, and brookite is 6 and that of O is 3, as required by stoichiometry. In amorphous nano-TiO_2, different coordination numbers of Ti and O may present, due both to greatly distorted coordination polyhedra and the lowered O-Ti coordination for near surface O. The coordination number distributions of Ti and O atoms were also calculated.

The Ti-O bond length was calculated for each Ti-O bond in a TiO_2 structure and the corresponding bond-length distribution was obtained. Similarly, the Ti-O-Ti and O-Ti-O bond-angles were also calculated, and the corresponding bond-angle distributions were obtained.

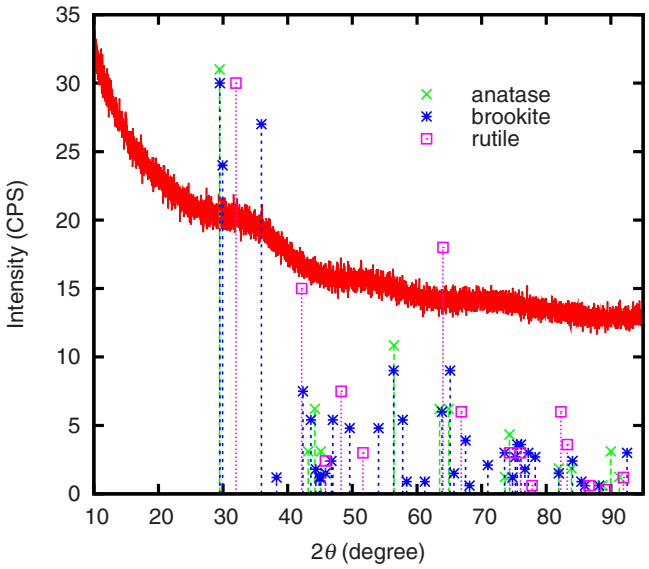

FIG. 1. (Color online) XRD pattern of nanometer-sized amorphous TiO_2. Diffraction data (in relative intensities) from the ICDD database for three ambient TiO_2 phases, anatase (Ref. 31), brookite (Ref. 32), and rutile (Ref. 33) are also shown for comparison.

IV. RESULTS AND DISCUSSION

A. Sample characterization

Figure 1 shows that there are no strong diffraction peaks in the XRD pattern of the synthesized TiO_2 sample. Given that only a few weak, broad humps (e.g., the one centered at ~35°) are present, the sample is "x-ray amorphous" (i.e., it cannot be identified as a anatase, brookite, or rutile).

TEM images show that the TiO_2 sample consists of TiO_2 aggregates (~0.2 μm in size) [Fig. 2(a)], which themselves are composed of clots of 2–3 nm TiO_2 primary nanoparticles [Fig. 2(b)]. Selected area electron diffraction of the sample [Fig. 2(a), inset] also shows no Bragg diffraction maxima.

The specific surface area of the sample determined by using the BET method is 433 m/g^2. This is equivalent to a size of ~3.5 nm in diameter assuming that all TiO_2 particles are spherical and that they are isolated from each other. Due to the surface contacts, the BET area must be less than the actual surface area of the analogously separated nanoparticles. Hence, the nanoparticle diameters must be somewhat smaller than 3.5 nm. These experimental results together establish that the synthesized TiO_2 sample is x-ray amorphous nano-TiO_2 with an average size of 2–3 nm in diameter.

B. Generation of structure models from reverse Monte Carlo simulations

The PDF, obtained from the experiments (Fig. 3), reflects the atomic correlations in the amorphous sample. The first intense peak at ~1.94 Å corresponds to the first O shell around a Ti atom. There are several PDF peaks at distances less than 7 Å, representing considerable short-range order in this nominally amorphous sample. At longer radial distances (>~8 Å), the PDF peaks are damped out, indicating lack of long-range order.

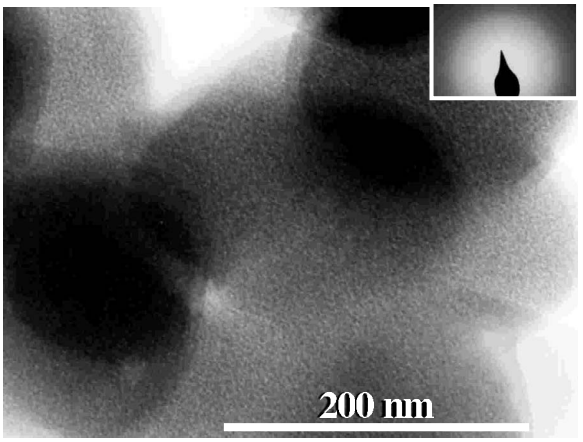

(a)

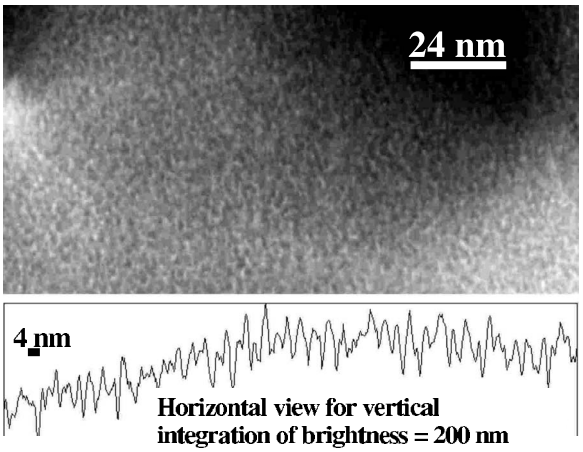

(b)

FIG. 2. TEM images of nanometer-sized TiO_2. (a) Low-resolution image showing aggregate sizes is ~0.2 μm in diameter. Inset: selected area electron-diffraction pattern. (b) High-resolution image showing primary particles is ~2–3 nm in diameter. Bottom: integration of contrast from TiO_2 nanoparticles.

Comparisons between some of our calculated and experimental PDFs are illustrated in Fig. 3. The calculated PDF of an as-constructed 2 nm anatase particle [Fig. 3(a), inset] deviates significantly from the experimental PDF [residue =41.05; Fig. 3(a)], while the calculated PDF of a 2 nm anatase particle obtained from MD simulation [Fig. 3(b), inset] is much closer to the experimental PDF [residue=6.10; Fig. 3(b)]. The calculated PDF of a 2 nm anatase [Fig. 3(c), inset] obtained from the RMC procedure (using a MD structure as its input) agrees very well with the experimental PDF [residue=1.52; Fig. 3(c)]. However, the agreement between the calculated PDF of a 2.5 nm anatase [Fig. 3(d), inset] obtained from a RMC (using MD structure input) with the experimental PDF is not as good [residue=3.15; Fig. 3(d)]. As noted above, additional trials showed that RMC using an as-constructed anatase nanoparticle as its input (i.e., not one from MD) is unable to generate a PDF consistent with experiment. These results demonstrate that RMC requires initial inputs from TiO_2 nanoparticle structures defined by MD simulations for adequate convergence, and that results are sensitive to particle size.

To further investigate the influences of the particle size and the specific phase of an input structure on the RMC output, MD simulations of 2 and 3 nm anatase, brookite, and rutile nanoparticles were performed to generate initial inputs for the RMC. Figure 4 shows the comparison between the experimental PDF and the PDF calculated from these RMC-derived structures. Figures 4(a) and 4(b) show that when using the MA potential set[18] for the MD, the RMC structure derived from a 2 nm anatase particle yields a PDF matching the experimental very well in terms of both the low residual (1.52) and the lack of structure (PDF peaks) at long radial distances (>~8 Å). Though the residuals for the RMC structures derived from 2 and 3 nm brookite particles are slightly lower (1.28 and 1.35, respectively), the RMC structures are more crystalline, as seen from the PDF peaks at radial distances >~8 Å. The RMC structures derived from 2 and 3 nm rutile particles and a 3 nm anatase particle both have higher residuals (>2.0) and significant PDF peaks at >~8 Å.

Figures 4(c) and 4(d) show the PDF of the RMC structures when using the KIM potentials[20] for the MD. For the 2 nm particles [Fig. 4(c)], the calculated PDF does not match the experimental one well (residuals >2.5). The calculated PDF peak at 3–4 Å is not well reproduced. For the 3 nm particles [Fig. 4(d)], it appears that the RMC structures from brookite and anatase (residuals of 1.69 and 1.73, respectively) are equally good in matching the experimental values.

We also attempted RMC with an input structure from MD of a 2 nm anatase particle with 308 H_2O molecules adsorbed on the surface. The RMC process was unable to generate PDF in good agreement with the experimental data in this case.

Hence, from RMC refinements, we obtain three RMC structures as candidate models for the nanometer-sized amorphous TiO_2. These are derived from the 2 nm anatase in Fig. 4(a) and the 3 nm brookite and 3 nm anatase in Fig. 4(d).

C. Selection of structure models by XANES spectra calculations

Experimental Ti *K*-edge XANES spectra of bulk anatase, bulk rutile, and amorphous nano-TiO_2 are shown in Fig. 5. The pre-edge peaks in the range of 4965–4975 eV are highly sensitive to the coordination environment of Ti atoms.[26] The pre-edge features will be used to select the best RMC structure models from the amorphous TiO_2 simulations. The analysis does not make use of the absorption edge position or features (i.e., peaks with energies >4980 eV) because they are not very specific of the Ti coordination environment (and hence the short-range order of Ti) due to the multiple scattering of Ti photon electrons by atoms in several neighboring shells.

For a more detailed examination, we calculated XANES spectra of bulk anatase and bulk rutile (Fig. 6) using varied conditions. Figure 6 shows that use of an atomic cluster radius of 7.0 Å allows both the MS and FDM methods to reproduce the pre-edge features of the bulk materials, though the FDM method gives better full spectra than the MS method. Since the muffin-tin approximation used in MS cal-

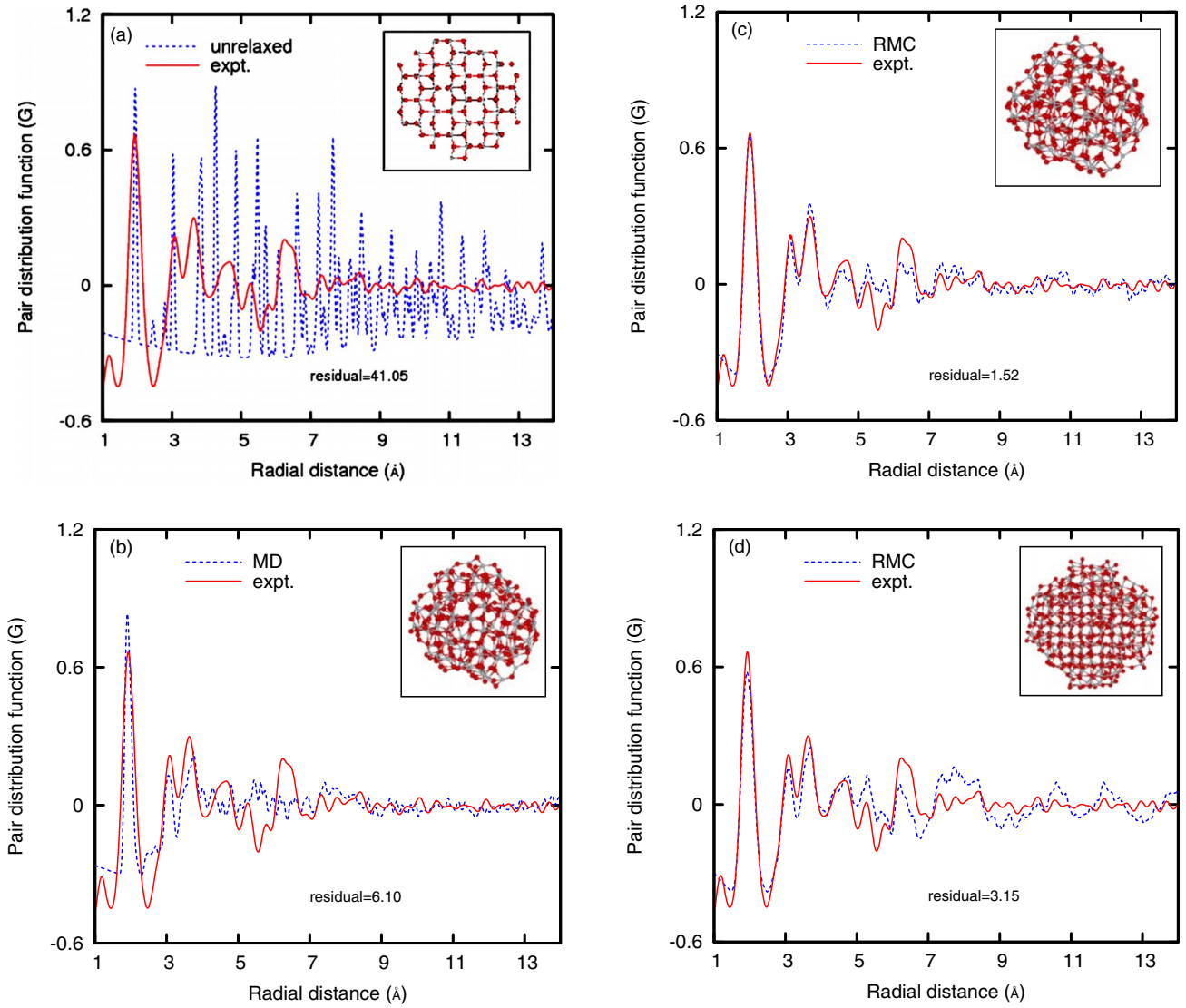

FIG. 3. (Color online) Comparison between experimental PDF of amorphous nano-TiO_2 and those calculated for anatase particles: (a) as-constructed (unrelaxed), 2 nm in diameter, after charge balancing; (b) from MD, 2 nm; (c) from RMC, 2 nm; and (d) from RMC, 2.5 nm. Input structures for the RMC were from MD using the MA interatomic potentials (Ref. 18). Insets show structure models used for the PDF calculations.

culations corresponds to a monopolar representation of the potential, it is insufficient for systems with low symmetry in the edge energy range.[23] Thus, the spectra calculated using a MS approach are not as close to the experimental spectra as those calculated via the FDM method, especially for anatase [Fig. 6(a)] which has a lower symmetry than rutile [Fig. 6(b)]. In bulk titania, peak $A1$ is from an electronic quadrupolar t_{2g} transition, $A3$ from the sum of a dipolar transition and a weak quadrupolar e_g transition, and B from a dipolar transition.[24,27] For bulk anatase [Fig. 6(a)], calculations using a smaller atomic radius of 5.6 Å were unable to generate pre-edge features that agreed well with the experimental data.

Figure 7 shows calculated XANES spectra for several RMC-derived structures. These include the structures starting from 2 and 3 nm anatase particles obtained via MD [Fig. 7(a)], and those starting from 2 nm anatase, brookite, and rutile particles obtained from MD [Fig. 7(b)]. Comparing the calculated spectra with the experimental spectra of amorphous nano-TiO_2 (Fig. 7), one sees that the structures from MD of nano-TiO_2 using the KIM potentials[20] generate larger pre-edge $A1$ peaks, which correspond to a larger proportion of four-coordinated Ti atoms in a material.[26] The calculated spectra for a 3 nm brookite (not shown) is similar to that for the 3 nm anatase shown in Fig. 7(a). In contrast, the RMC structures derived from MD of 2 nm TiO_2 nanoparticles using the MA potentials[18] produce larger pre-edge $A2$ peaks (which are associated with five-coordinated Ti atoms in a material[26]) with positions and intensities in good agreement with the experimental [Fig. 7(a)].

Combining both the RMC results (above) and the XANES simulations, we conclude that the RMC structure derived from a 2 nm anatase particle by MD using the MA potentials [Figs. 3(c) and 4(a)] best describes both the WAXS and XAS data. It also appears that the MA set of potentials[18] is supe-

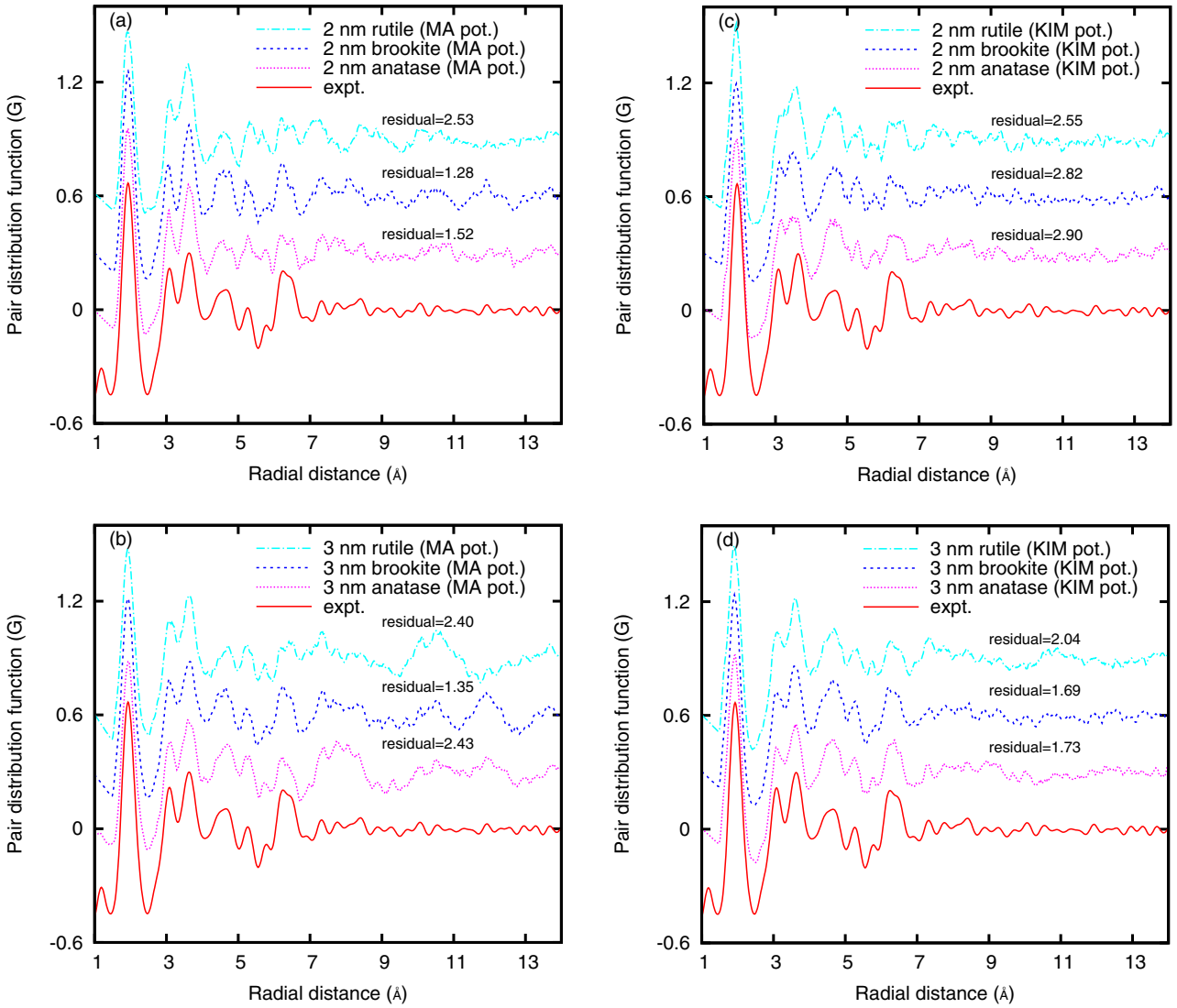

FIG. 4. (Color online) Comparison between experimental PDF of amorphous nano-TiO_2 and those calculated from RMC structures. Input structures for the RMC were from MD of [(a) and (c)] 2 nm and [(b) and (d)] 3 nm TiO_2 particles using [(a) and (b)] the MA interatomic potentials (Ref. 18) and [(c) and (d)] the KIM potentials (Ref. 20).

rior to the KIM set[20] for MD simulations of these types of TiO_2 materials.

D. Analyses of structure models of amorphous nano-TiO_2

We now analyze further the structural features of two models, the one that best describes the WAXS or XAS data [Fig. 3(c); model 1] and the one from RMC of a 3 nm anatase by MD using the KIM potentials [Fig. 4(d); model 2]. Though the PDF of model 2 is also close to the experimental data [Fig. 4(d)], the predicted XANES pre-edge feature of model 2 is quite different from the experimental spectra [Fig. 7(a)], and we wish to determine the basis for this divergence. Figures 8(a) and 8(b) show the three-dimensional (3D) and cross-section views of structure model 1; Figs. 8(c) and 8(d) show those of structure model 2.

Figures 8(a) and 8(b) (model 1) reveal that the nano-TiO_2 particle has a strained anataselike crystalline core, with a dimension of ~2 unit cells, and a highly distorted outer

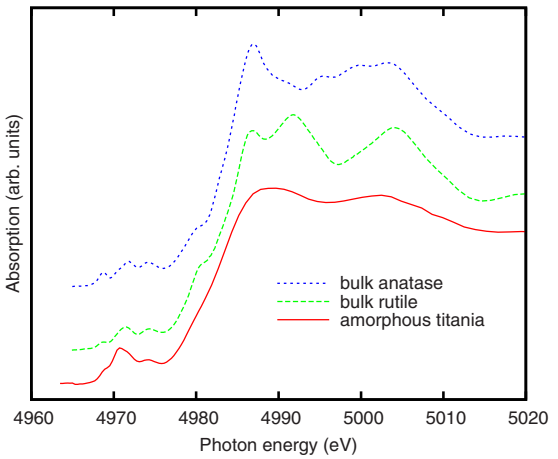

FIG. 5. (Color online) Experimental XANES spectra of bulk anatase, bulk rutile, and amorphous nano-TiO_2.

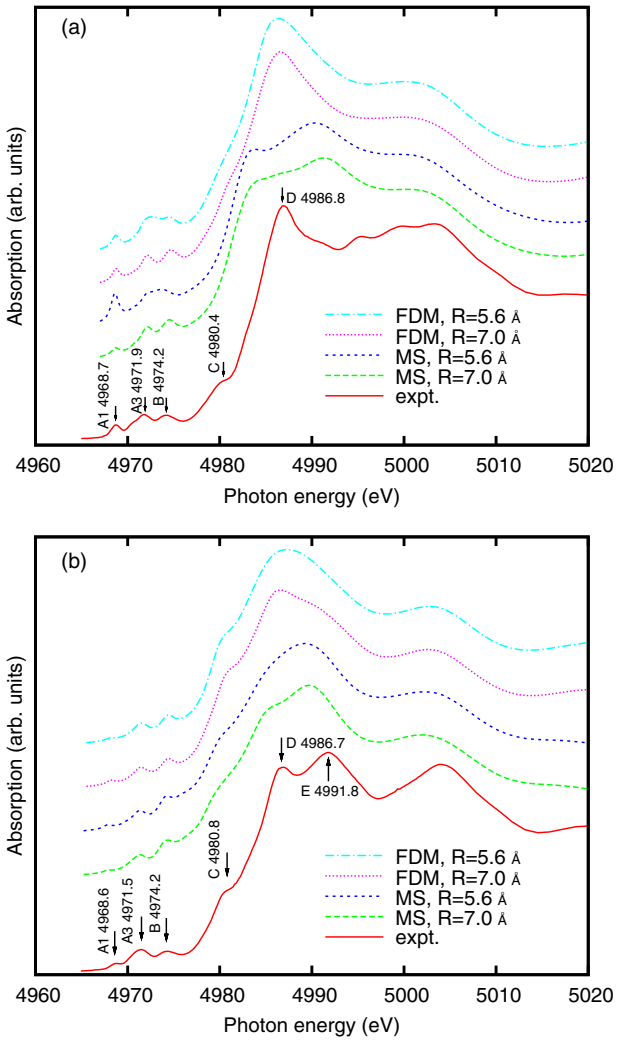

FIG. 6. (Color online) Comparison of calculated XANES spectra of (a) bulk anatase and (b) bulk rutile with the experimental spectra. Finite difference method and multiple-scattering method were used in the calculations with atomic cluster radii (R) of 5.6 and 7.0 Å. Characteristic peaks are shown on the experimental spectra.

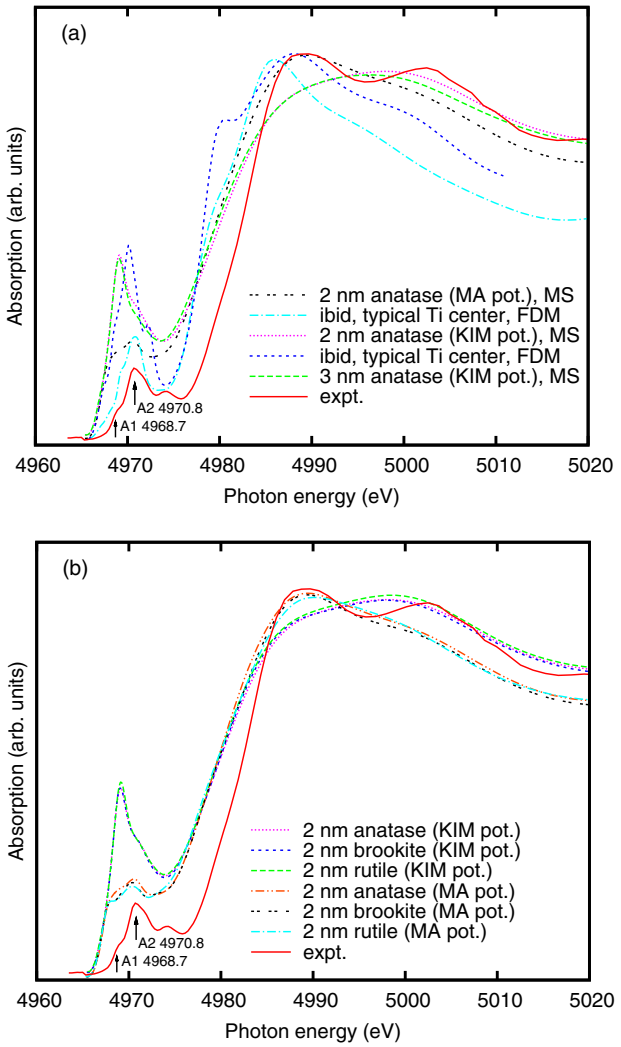

FIG. 7. (Color online) Comparison of calculated XANES spectra of nano-TiO_2 with the experimental spectra of amorphous nano-TiO_2. MS method (cluster radius, 7.0 Å) and FDM method (cluster radius, 4.0 Å) were used in the calculations. Structure models for the spectra calculations were from RMC with input structures from MD of (a) 2 and 3 nm anatase particles, and (b) 2 nm anatase, brookite, and rutile particles (all with MS method). The MA (Ref. 18) and KIM (Ref. 20) interatomic potentials were used in the MD.

shell, ~2–4 atomic layers thick. The density of the particle is 3.74 g/cm^3, lower than that of bulk anatase (3.90 g/cm^3). Due to the small dimension of the strained core, x-ray beams are unable to generate coherent reflections in a diffraction experiment. Thus, the synthesized sample appears x-ray amorphous. The pre-existence of the anatase-like core in the particles may be critical to the development of the amorphous titania into single-phase nanoanatase during heat treatment. In contrast, the structure shown in Figs. 8(c) and 8(d) (model 2) has no crystalline order.

Based on RMC of bulk structure models, Petkov *et al.*[16] concluded that alkoxide-derived amorphous TiO_2 has a brookitelike structure. Using a bulk structure model neglects any size effects on the structure. As such, no difference can be made between particle surfaces and interiors, and thus the obtained structure model could be far from realistic.

Figure 9 compares all results for the two structure models. An obvious difference in the partial radial-distribution function for the two models [Figs. 9(a) and 9(b)] is that g(TiTi) is less resolved at ~3.3 Å for model 2 [Fig. 9(b)] than for model 1 [Fig. 9(a)] due to the noncrystalline structure in model 2. The coordination numbers of Ti, CN(TiO), for model 1 and model 2 are, respectively, 5.3 and 4.1 at the first O shell [Figs. 9(a) and 9(b)]. This indicates that the first model TiO_2 is comprised mainly of distorted Ti-O octahedra (CN=6) and/or pentahedra (CN=5) rather than tetrahedra (CN=4), though the Ti-O bond lengths all distribute around 1.94 Å in the two models [Fig. 9(c)]. More detailed analysis shows that, in model 1 [Fig. 9(d)] some of the Ti atoms are coordinated by four O atoms, a few by seven O atoms, but most Ti atoms are coordinated by five and six O atoms. In model 2 [Fig. 9(d)], most Ti atoms are coordinated by four O atoms, some by five atoms, and a few by three and six atoms.

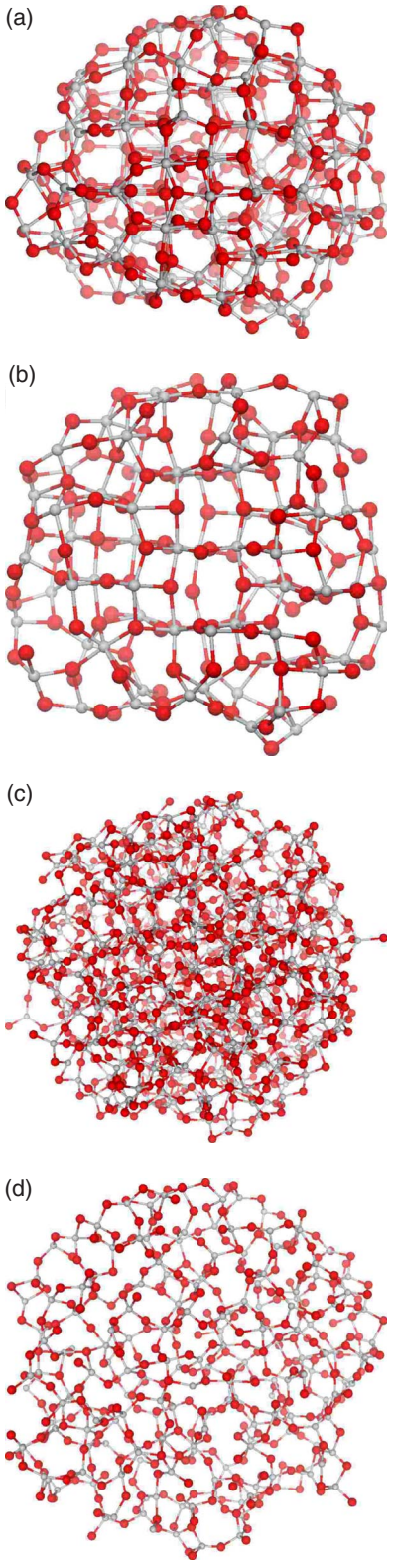

FIG. 8. (Color online) Structure of a TiO_2 nanoparticle generated by RMC of [(a) and (b)] an ~2 nm anatase particle (model 1), and [(c) and (d)] an ~3 nm anatase particle (model 2). (b) and (d) are cross-section views. Input structures for the RMC were from MD using [(a) and (b)] the MA interatomic potentials (Ref. 18) and [(c) and (d)] the KIM potentials (Ref. 20). Ti: smaller balls; O: bigger balls.

Most O atoms are coordinated by two or three Ti atoms in model 1 [Fig. 9(e)] and two Ti atoms in model 2 [Fig. 9(e)].

In a previous study, Fernandez-Garcia *et al.*[15] concluded that five coordinated Ti atoms are present in amorphous TiO_2 based on the pre-edge feature in the XANES spectra. However, their EXAFS fitting showed that Ti atoms are coordinated by 6.2–6.7 oxygen atoms (two shells of O atoms) at a Ti-O distance of 1.71–1.92 Å. Their EXAFS results appear inconsistent with their XANES results and are different than our results for model 1.

Figures 9(f) and 9(g) show the bond-angle distributions in the two models. The distributions in model 1 can be seen as broadening and overlapping the distributions in bulk anatase due to distortions of the Ti-O octahedra in the nanoparticles and truncations of the octahedra at the particle surfaces. The distributions in model 2 deviate significantly from those in bulk anatase. This is expected because the model 2 is mainly comprised of Ti-O tetrahedra in which O-Ti-O angles average around 109°.

The surface and the interior of a TiO_2 nanoparticle are different in structure [Figs. 8(a) and 8(b)]. Figure 10 shows structure characteristics of the surface (the distorted shell) and the core of model 1. From the radial distribution function [Fig. 10(a)], it is seen that most Ti-O bonds in the core are longer that those in the shell, indicating bond contraction at the surface due to interrupted coordination. This follows from bond valence analysis, i.e., smaller Ti-O CN is consistent with shorter Ti-O bonds. The peak Ti-O bond length of the whole particle is also shorter than that of bulk anatase due to the compression from the effective surface pressure due to small size.[28] The reductions in coordination numbers of Ti and O atoms at the surface are clearly seen in Figs. 10(b) and 10(c), while in the core, the coordination numbers are close to those in bulk anatase. Previous studies concluded that the reduction in coordination number of Ti atoms in ultrafine[9,10] or amorphous[11] titania materials is mainly located on the particle surfaces. Our results are consistent with this. The bond-angle distributions [Figs. 10(d) and 10(e)] show that those of the whole nanoparticle are largely contributed by the surface atoms as the distributions from the surface approximately double those from the core. These results demonstrate that the structure features of the amorphous TiO_2 nanoparticles are determined dominantly by the surface structure, which is a result of the relaxation of the surface coordination polyhedra to incomplete coordination by oxygen and added degrees of angular freedom.

It is clear now that it is the difference in the average coordination number of Ti in mode 1 (CN 5.3) and model 2 (CN 4.1) that generated quite different pre-edge features in the simulated XANES spectra [Fig. 7(a)]. Model 1 is more realistic because it reproduced well both the WAXS and XAS data, and it is consistent with the majority of past work. This model [Figs. 8(a) and 8(b)], however, provides us with a more detailed understanding of the atomic arrangements in alkoxide-derived nanometer-sized amorphous TiO_2 than previously described. The structure model will be used for future computational study of the mechanical, photonic, and catalytic properties of nanometer-sized amorphous titania.

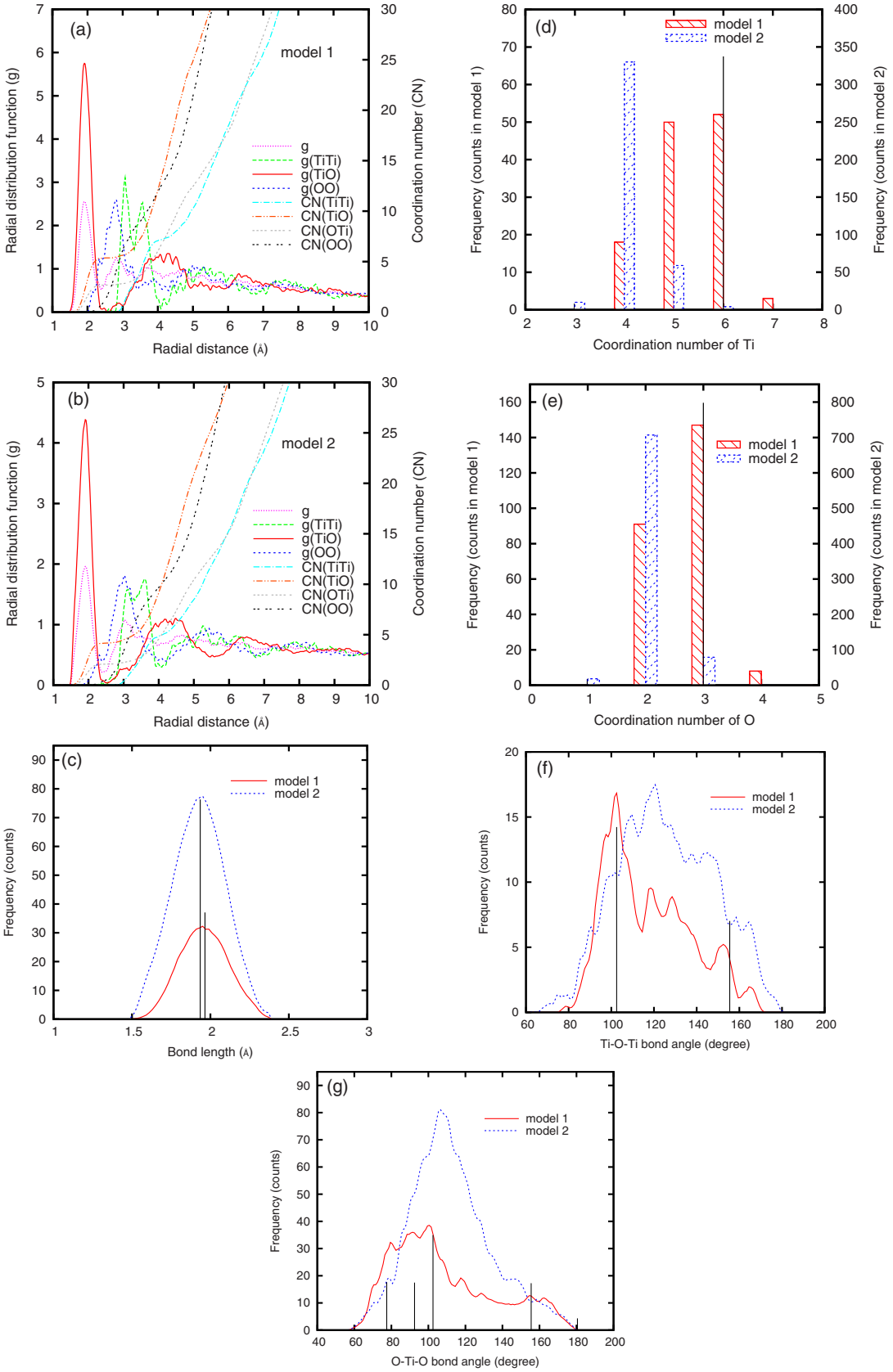

FIG. 9. (Color online) Structural characteristics of amorphous nano-TiO_2. (a) RDF (g) and CN of model 1. g—total RDF; $g(AB)$—partial RDF of B around A; CN(AB)—CN of B around A. (b) RDF and CN of model 2. (c) Bond length distribution. (d) Coordination number distribution of Ti. (e) Coordination number distribution of O. (f) Ti-O-Ti bond-angle distribution. (g) O-Ti-O bond-angle distribution. Vertical lines represent the corresponding values in bulk anatase (shown in relative magnitudes).

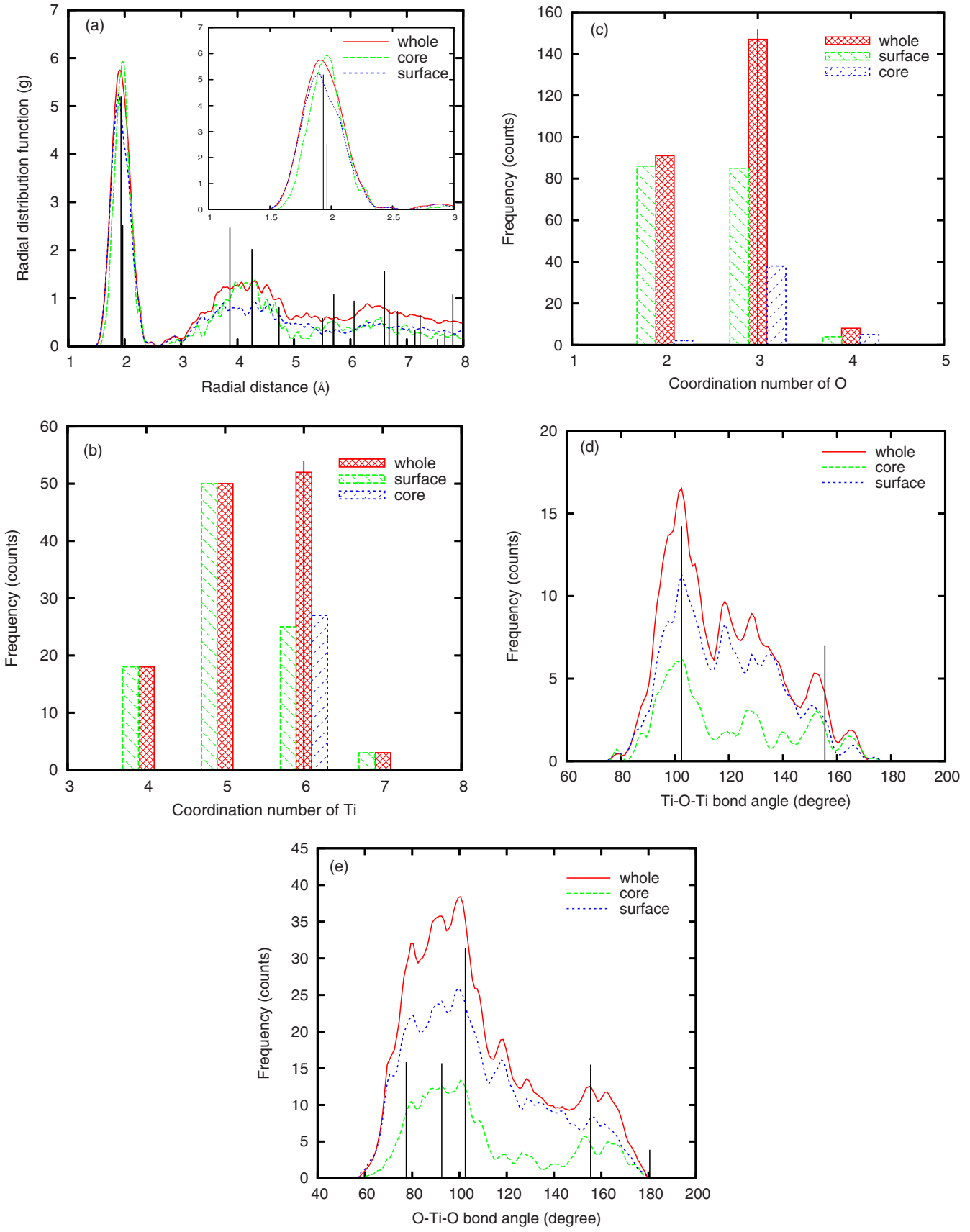

FIG. 10. (Color online) Structural characteristics of the surface, core, and whole amorphous nano-TiO_2 particle (model 1). (a) RDF of O around Ti. (b) Coordination number distribution of Ti. (c) Coordination number distribution of O. (d) Ti-O-Ti bond-angle distribution. (e) O-Ti-O bond-angle distribution. Vertical lines represent the corresponding values in bulk anatase (shown in relative magnitudes).

V. CONCLUSIONS

We studied alkoxide-derived x-ray amorphous titania composed of ~2 nm TiO_2 nanoparticles using combined experimental determination and computational modeling. Results show that the nanoparticles have a highly distorted shell and a strained anataselike core, with an average Ti-O coordination number of 5.3. The reduction in the coordination number is mainly due to Ti atoms located in the outer shells of the nanoparticles. Most Ti-O bonds (peaked at 1.940 Å) are shorter than those in bulk anatase (four bonds, 1.937 Å; two bonds, 1.965 Å; average, 1.946 Å),[29] which is due to the bond contractions in the distorted surface shells. Because of the existence of the anataselike cores in the nanoparticles, this type of amorphous nano-TiO_2 serves as an ideal precursor for the synthesis of single-phase nanocrystalline anatase via heat treatment.[2] Core-shell structures in ultrafine nanoparticles (distorted shells plus strained crystalline cores) may be common in many materials, and have also been observed in small ZnS nanoparticles.[30]

ACKNOWLEDGMENTS

Synchrotron experiments were performed at beamlines 11-ID-C (WAXS), 20-BM-B (XAS), and 5-BM-D (XAS), Advanced Photon Source, Argonne National Laboratory. We thank R. Yen, Q. Ma, and M. Balasubramanian for assistance in the beamline experiments. Computations were carried out in the Geochemistry Computer Cluster, Lawrence Berkeley National Laboratory. Y. Joly is thanked for help in using the FDMNES program. Financial support was provided by the U.S. Department of Energy (Grant No. DE-FG03-01ER15218) and the National Science Foundation (Grant No. EAR-0123967).

*Corresponding author; heng@eps.berkeley.edu

[1] L. Gao and Q. Zhang, Scr. Mater. **44**, 1195 (2001).
[2] H. Zhang, M. Finnegan, and J. F. Banfield, Nano Lett. **1**, 81 (2001).
[3] H. Zhang and J. F. Banfield, Am. Mineral. **84**, 528 (1999).
[4] H. Zhang and J. F. Banfield, J. Mater. Res. **15**, 437 (2000).
[5] H. Zhang and J. F. Banfield, J. Phys. Chem. B **104**, 3481 (2000).
[6] H. Zhang and J. F. Banfield, J. Phys. Chem. C **111**, 6621 (2007).
[7] H. Zhang and J. F. Banfield, J. Mater. Chem. **8**, 2073 (1998).
[8] H. Zhang and J. F. Banfield, Chem. Mater. **14**, 4145 (2002).
[9] L. X. Chen, T. Rajh, Z. Wang, and M. C. Thurnauer, J. Phys. Chem. B **101**, 10688 (1997).
[10] L. X. Chen, T. Rajh, W. Jager, J. Nedeljkovic, and M. C. Thurnauer, J. Synchrotron Radiat. **6**, 445 (1999).
[11] V. Luca, S. Djajanti, and R. F. Howe, J. Phys. Chem. B **102**, 10650 (1998).
[12] K. L. Yeung, A. J. Maira, J. Stolz, E. Hung, N. K.-C. Ho, A. C. Wei, J. Soria, K.-J. Chao, and P. L. Yue, J. Phys. Chem. B **106**, 4608 (2002).
[13] H. Yoshitake, T. Sugihara, and T. Tatsumi, Phys. Chem. Chem. Phys. **5**, 767 (2003).
[14] H. Yoshitake, T. Sugihara, and T. Tatsumi, Chem. Mater. **14**, 1023 (2002).
[15] M. Fernandez-Garcia, C. Belver, J. C. Hanson, X. Wang, and J. A. Rodriguez, J. Am. Chem. Soc. **129**, 13604 (2007).
[16] V. Petkov, G. Holzhuter, U. Troge, Th. Gerber, and B. Himmel, J. Non-Cryst. Solids **231**, 17 (1998).
[17] B. Gilbert, F. Huang, H. Zhang, G. A. Waychunas, and J. F. Banfield, Science **305**, 651 (2004).
[18] M. Matsui and M. Akaogi, Mol. Simul. **6**, 239 (1991).
[19] P. K. Naicker, P. T. Cummings, H. Zhang, and J. F. Banfield, J. Phys. Chem. B **109**, 15243 (2005).
[20] D.-W. Kim, N. Enomoto, and Z.-e. Nakagawa, J. Am. Ceram. Soc. **79**, 1095 (1996).
[21] W. Smith and T. R. Forster, *The DL_POLY v2.13 User Manual* (Daresbury Laboratory, Warrington, 2001).
[22] Y. Joly, *FDMNES User's Guide* (Institute Néel, CNRS, Grenoble Cedex, 2007).
[23] Y. Joly, Phys. Rev. B **63**, 125120 (2001).
[24] Y. Joly, D. Cabaret, H. Renevier, and C. R. Natoli, Phys. Rev. Lett. **82**, 2398 (1999).
[25] P. Vashishta, R. K. Kalia, J. P. Rino, and I. Ebbsjo, Phys. Rev. B **41**, 12197 (1990).
[26] F. Farges, G. E. Brown, Jr., and J. J. Rehr, Geochim. Cosmochim. Acta **60**, 3023 (1996).
[27] D. Cabaret, Y. Joly, H. Renevier, and C. R. Natoli, J. Synchrotron Radiat. **6**, 258 (1999).
[28] S. H. Tolbert and A. P. Alivisatos, Annu. Rev. Phys. Chem. **46**, 595 (1995).
[29] S.-D. Mo and W. Y. Ching, Phys. Rev. B **51**, 13023 (1995).
[30] H. Zhang, B. Gilbert, F. Huang, and J. F. Banfield, Nature (London) **424**, 1025 (2003).
[31] International Center for Diffraction Data, Powder Diffraction File ICDD-PDF2, Reference Code No. 00-021-1272 (Newton Square, PA, 2003).
[32] International Center for Diffraction Data, Powder Diffraction File ICDD-PDF2, Reference Code No. 00-029-1360 (Newton Square, PA, 2003).
[33] International Center for Diffraction Data, Powder Diffraction File ICDD-PDF2, Reference Code No. 00-021-1276 (Newton Square, PA, 2003).